Evaluation of Multivalent, Functional Polymeric Nanoparticles for Imaging Applications

Monica Shokeen,[†,▽] Eric D. Pressly,[⊥,∥,▽] Aviv Hagooly,[†] Alexander Zheleznyak,[†] Nicholas Ramos,[†] Ashley L. Fiamengo,[†] Michael J. Welch,[†,§] Craig J. Hawker,[⊥,∥,¶,*] and Carolyn J. Anderson[†,‡,§,*]

[†]Mallinckrodt Institute of Radiology, [‡]Department of Chemistry, [§]Department of Biochemistry and Molecular Biophysics, Washington University, St. Louis, Missouri 63110, United States, [⊥]Materials Research Laboratory, [∥]Materials Department, and [¶]Department of Chemistry and Biochemistry, University of California, Santa Barbara, California 93106, United States. [▽] These authors contributed equally to this work.

Nanotechnology offers a range of unique opportunities in the fields of diagnostic and therapeutic medical applications with significant advances in the design and application of tailored nanoparticle-based drug delivery platforms, paving the way for further progress in cellular biology and clinical and imaging sciences. A guiding principle in this rapidly growing biomedical area is the ability of nanoparticles to mimic the high affinity, multivalent interactions that exist in cellular systems in order to produce highly efficient, diagnostic and therapeutic synthetic systems.[1−8] While there are currently a limited number of nanoparticle-based drug delivery systems approved by the U.S. Federal Drug Administration for treatment,[9] a wide range of self-assembled, covalent, and organic/inorganic composite structures are being actively studied.[10−17] In each case, comparison with the corresponding small molecules demonstrates that the nanoparticle systems offer optimal pharmokinetics/circulation half-life, increased tolerance toward enzymatic degradation, greater physical and chemical stability, and slower drug release kinetics at the target site.[12]

Ideally, nanoparticles as drug delivery or diagnostic agents must bind specifically to their targets to differentiate between normal and diseased cells and to avoid systemic toxicity. To selectively target diseased cells, nanoparticles are often conjugated with moieties such as peptides and antibodies that specifically bind to overexpressed biomarkers on the diseased cells. As a result, these functionalized nanoparticle platforms increase the accumulation and efficacy of the diagnostic and therapeutic agents at the target sites. Receptor-based strategies are particularly valuable as many cell surface receptors are up-regulated in cancerous cells and other disease states, providing a clear marker for drug delivery systems with the nanoparticles' ligand concentration being important in targeting.[18]

While nanoparticles confer many advantages over small molecules, problems associated with such engineered agents still need to be addressed. For instance, the concentration of moieties conjugated to the surface of the nanoparticles must be optimized. A high payload of the moieties is correlated with an increased selective uptake of the agent in diseased cells. At too high a concentration, however, the payload can trigger an abnormal reticuloendothelial system (RES) response and rapid blood clearance, both of which adversely affect the agent's viability as "stealthy" medicinal agents.[11,19]
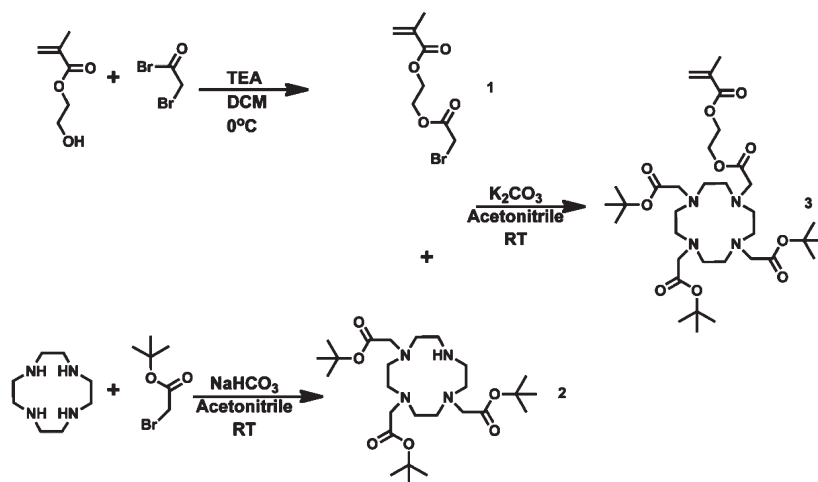
The goal of this study is to develop a synthetic strategy for accurate loading of

ABSTRACT A series of multivalent, functional polymer nanoparticles with diagnostic/imaging units and targeting ligands for molecular targeting were synthesized with the loading of the chain-end-functionalized GRGDS peptide targeting sequence (model system based on integrin $\alpha_v\beta_3$) ranging from 0 to 50%. Accurate structural and functional group control in these systems was achieved through a modular approach involving the use of multiple functionalized macromonomer/monomer units combined with living free radical polymerization. *In cellulo* results show an increase in uptake in $\alpha_v\beta_3$ integrin-positive U87MG glioblastoma cells with increasing RGD loading and a possible upper limit on the effectiveness of the number of RGD peptides for targeting $\alpha_v\beta_3$ integrin. Significantly, this increased targeting efficiency is coupled with *in vivo* biodistribution results, which show decreased blood circulation and increased liver uptake with increasing RGD loading. The results demonstrate the importance of controlling ligand loading in order to achieve optimal performance for therapeutic and imaging applications for multivalent nanoparticle-based systems.

KEYWORDS: polymeric nanoparticles · click chemistry · cellular uptake · pharmacokinetics

Scheme 1. Synthetic scheme for DOTA methacrylate building block, 3.
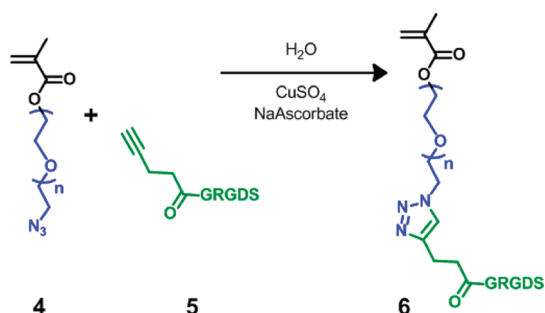
Scheme 2. Synthesis of the functionalized RGD-PEGMA macromonomer, 6.

targeting moieties and diagnostic units onto a polymeric nanoparticle scaffold and to exploit this high level of control to understand and evaluate the competing effects of ligand loading on nanoparticle binding affinity and uptake *in cellulo* compared to the effect on their pharmacokinetic properties. Here we demonstrate that the modular and tunable nature of the synthetic approach to these multifunctional comb nanoparticle (CNP) carriers allows for the design of systems with increased specific integrin binding and cellular uptake, optimal blood retention, and RES response based on an intermediate loading of targeting peptides. Of the many molecular targets available, $\alpha_v\beta_3$, a well-studied type of integrin upregulated in tumor angiogenesis, metastasis, inflammation, certain cardiovascular abnormalities, and bone resorption,[20] was selected as a model system for evaluation. To synthesize agents capable of detecting $\alpha_v\beta_3$, small peptides containing the amino acid sequence Arg-Gly-Asp (RGD), which bind to $\alpha_v\beta_3$ with high affinity, were linked to the polymeric backbone of nanoparticles at various concentrations. Notably, the novel modular and tunable synthetic approach ensures accurate control over conjugation of RGD peptides to the backbone. Finally, this series of RGD–comb nanoparticles were radiolabeled with ^{64}Cu ($T_{1/2}$ = 12.7 h, β^+ = 17.86%), a positron emitter commonly used in

positron emission tomography (PET), *via* the DOTA (1,4,7,10-tetraazacyclododecane-1,4,7,10-tetraacetic acid) chelator for evaluations *in cellulo* and *in vivo*.

RESULTS AND DISCUSSION

Synthesis of Comb Copolymers. Herein we describe the synthesis, *in cellulo*, and pharmacokinetic *in vivo* evaluation of a class of multifunctional nanoparticles as a model system for developing structure/bioperformance relationships. Using the binding of RGD to the integrin $\alpha_v\beta_3$ as a prototypical system, well-defined amphiphilic graft copolymers and associated comb nanoparticles (CNPs) having a controlled number of RGD peptide targeting moieties were prepared. The modular approach used in this study is based on four important building blocks: (a) poly(ethylene glycol) (PEG) as a hydrophilic, protein-resistant unit;[21,22] (b) methyl methacrylate as a hydrophobic backbone which controls self-assembly; (c) 1,4,7,10-tetraazacyclododecane-*N*,*N'*,*N''*,*N'''*-tetraacetic acid (DOTA) as a chelator for imaging with the positron emitter ^{64}Cu ($T_{1/2}$ = 12.7 h, β^+ = 17.86%); and (d) GRGDS as a linear targeting peptide. The key to this strategy is the preparation of functional monomers and macromonomers, where incorporation of the desired targeting ligands and diagnostic units into these target structures allows for a more reproducible level of incorporation during living free radical polymerization. This degree of control also permits the spatial location of the building blocks along the polymer backbone to be manipulated, important for both nanoparticle self-assembly and activity of the various components (*i.e.*, targeting moieties should be at the surface).[18]

The DOTA methacrylate, **3**, was synthesized as shown in Scheme 1, from the bromomethylacyl methacrylate derivative, **1**, and the tris-functionalized cyclen derivative, **2**, allowing direct incorporation of the diagnostic ^{64}Cu–DOTA units in the interior of the nanoparticle after deprotection and ^{64}Cu insertion. The
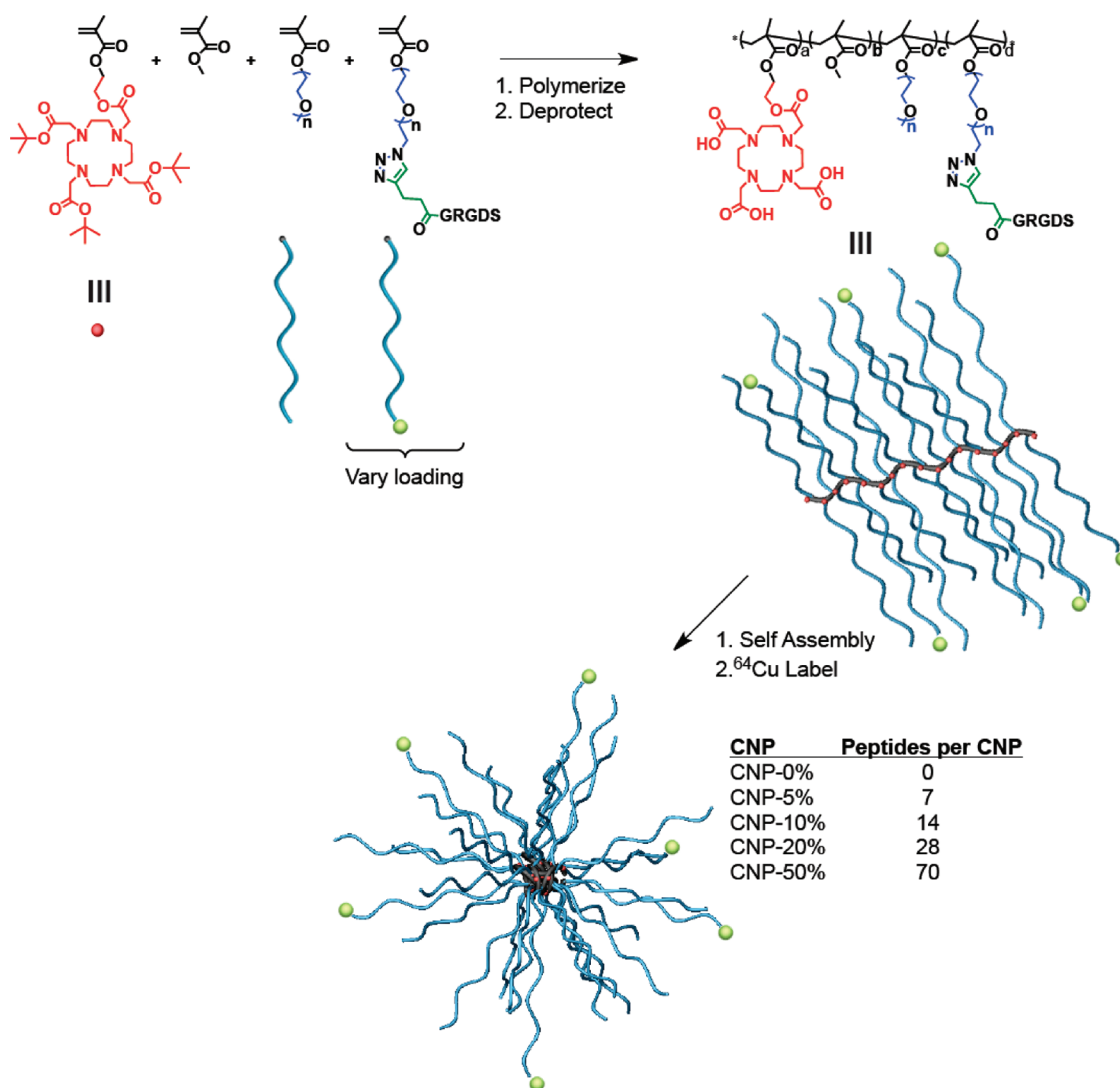
Scheme 3. Synthesis of functionalized comb copolymers by RAFT polymerization and their assembly into CNPs.

CNP	Peptides per CNP
CNP-0%	0
CNP-5%	7
CNP-10%	14
CNP-20%	28
CNP-50%	70

TABLE 1. Structural Features of RGD-Functionalized Comb Copolymers

polymer	M_n (GPC)	PDI (GPC)	M_n (NMR)	CNP	CNP diameter (nm)	RGDs per CNP
0% RGD	120 kDa	1.3	140 kDa	CNP-0%	20.4	0
5% RGD	125 kDa	1.3	141 kDa	CNP-5%	22.0	7
10% RGD	130 kDa	1.3	141 kDa	CNP-10%	21.8	14
20% RGD	120 kDa	1.3	142 kDa	CNP-20%	22.9	28
50% RGD	110 kDa	1.3	145 kDa	CNP-50%	20.9	70

RGD−PEG macromonomer, **6**, was synthesized in two steps from a heterobifunctional PEG containing a hydroxyl and an azide chain end. The initial step involved introduction of the methacrylate functionality at the hydroxyl end of the heterobifunctional PEG through reaction with methacryloyl chloride to give **4**. Following this, the acetylene-derivatized GRGDS peptide, **5**, was attached using Cu(I) click chemistry, which proved to be orthogonal to the functional groups displayed on

peptides as well as the polymerizable methacrylate unit, giving the desired macromonomer, **6**, in excellent yield and purity (Scheme 2).[23−25] Although a previous report by Dechantsreiter et al.[26] points to improved affinity exhibited by cyclic peptides, in vitro experiments performed in our laboratory demonstrated that, although the lactam-cyclized peptide, c(RGDyK), had increased binding affinity for $\alpha_v\beta_3$ (3.7 nM) over the linear peptide (GRGDS, 15.9 nM), GRGDS had improved specificity for $\alpha_v\beta_3$ compared to other integrins (c(RGDyK), $\alpha_v\beta_5$: 171 nM, $\alpha_{IIb}\beta_3$: 0.11 nM; GRGDS, $\alpha_v\beta_5$: >5000 nM, $\alpha_{IIb}\beta_3$: 873 nM).[27] Additionally, the cellular uptake was comparable for the cyclized and linear peptides.[27]

Copolymerization of these well-defined monomers with varying amounts of PEG methacrylate and methyl methacrylate comonomers allows the preparation of a library of functionalized comb copolymers. The polymerizations were performed to ca. 50% conversion, which gives low polydispersity and controlled molecular weight
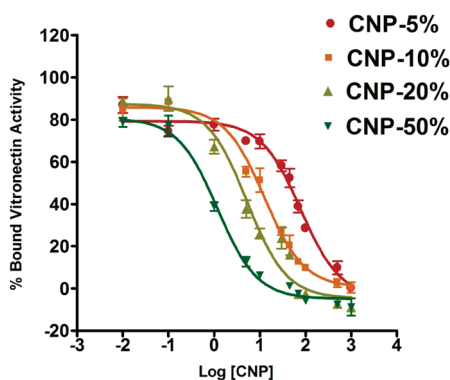
Figure 1. IC$_{50}$ binding curves for RGD−CNPs for the human integrin $\alpha_v\beta_3$, obtained by competition with biotinylated vitronectin.

TABLE 2. Integrin Binding (IC$_{50}$) Results from the RGD−CNP Series from an Isolated Integrin Binding Assay in Competition with Vitronectin ($\alpha_v\beta_3$ and $\alpha_v\beta_5$) and Fibronectin ($\alpha_{IIb}\beta_3$)

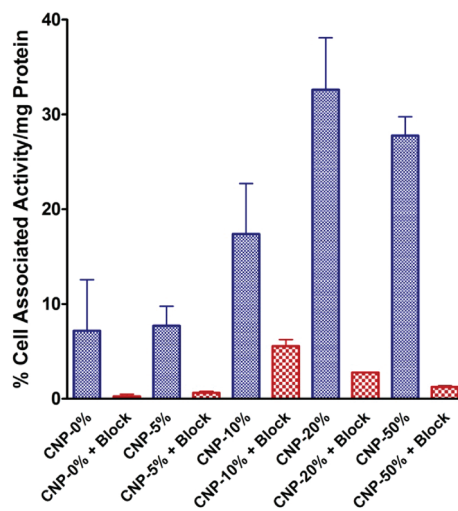| CNPs	number of peptides per CNP	IC$_{50}$ $\alpha_v\beta_3$ (nM)	IC$_{50}$ $\alpha_v\beta_5$ (nM)	IC$_{50}$ $\alpha_{IIb}\beta_3$ (nM)
5%	7	78.46	>1000	>1000
10%	14	12.48	>1000	>1000
20%	28	5.21	>1000	>1000
50%	70	1.08	>1000	>1000
0% (nontargeted) control	0	>1000	>1000	>1000

Figure 2. Cell-associated ^{64}Cu−RGD−CNPs at 37 °C at 30 min time point in U87MG glioblastoma cells as a function of RGD content. Blocking was carried out by coincubation with 1 μM nonradioactive nanoparticle solution (500 μL total volume).

materials where the level of incorporation of the functionalized monomers agrees with the feed ratios.[28−30] By controlling the relative hydrophobic/hydrophilic balance of the copolymers through the ratio of methyl methacylate and PEG units, assembly into CNPs was observed and nanoparticles with approximately the same size (∼22 nm), irrespective of the level of incorporation of the RGD units obtained (Table 1). This allows variations with respect to CNP size to be eliminated and direct comparison between the samples with 0% RGD, 5% RGD, 10% RGD, 20% RGD and 50% RGD −CNPs having approximately 0, 7, 14, 28, and 70 RGD's per CNP to be made. As has been previously shown, the stability of the ^{64}Cu-labeled-CNPs were tested in serum and cell culture conditions up to 48 h and no dissociation of ^{64}Cu or degradation of the CNPs was observed.[28] In our previous work, we showed the effects of PEO length on particle biodistribution as well as polymer assembly into core−shell nanoparticles by DLS, SANS and CryoTEM.[28] The nanoparticle nature of our system provides for longer circulation times than similar random copolymer systems developed by Kopeček et al.[31]

***In Vitro* Evaluation of $\alpha_v\beta_3$ Targeted CNPs by Isolated Integrin Binding Assays.** In evaluating the biological activity of RGD-functionalized CNPs toward $\alpha_v\beta_3$, the effect of multivalency on integrin binding affinity was assessed by performing isolated integrin binding assays. CNPs with variable levels of RGD attachment were evaluated for their binding affinity and specificity toward the integrins $\alpha_v\beta_3$, $\alpha_v\beta_5$, and $\alpha_{IIb}\beta_3$ in heterologous competitive binding experiments with biotinylated vitronectin ($\alpha_v\beta_3$, $\alpha_v\beta_5$) and fibronectin ($\alpha_{IIb}\beta_3$) as the competitive natural ligand, respectively. Nonlinear regression was used to fit the binding curves and calculate inhibitory concentration values of 50% (IC$_{50}$), with the $\alpha_v\beta_3$ binding kinetics following a classic sigmoid path that could be fit with a nonlinear regression curve (Figure 1). The results demonstrate a *ca.* 75-fold increase in $\alpha_v\beta_3$ binding between the 5% RGD−CNPs (IC$_{50}$ = 78.46 nM) and 50% RGD−CNPs (IC$_{50}$ = 1.08 nM), which is in contrast to the number of RGD targeting ligands where the increase is only a factor of 10.

The 10 and 20% RGD−CNPs had intermediate IC$_{50}$ values of 12.48 and 5.21 nM, respectively, with the significant finding being the nonlinear nature of the relationship between the IC$_{50}$ and the number of peptides (Table 2). The results indicate that increasing the number of targeting peptides per CNP translates to increased binding affinity to the integrin, with the nontargeted control CNP showing no appreciable binding to $\alpha_v\beta_3$ (Table 2). For example, doubling the number of peptides from the 5% sample to the 10% sample leads to a 6-fold improvement in binding, while a 10-fold increase in peptide attachment corresponds to a 75-fold improvement in the IC$_{50}$ value. This enhancement in the binding affinity can be attributed to both the multivalent nature of the nanoparticle design as well as the increased availability of the targeting peptides at the surface of the nanoparticle.

The RGD−CNPs were also screened against the integrins $\alpha_v\beta_5$ and $\alpha_{IIb}\beta_3$, found on macrophages and blood platelets, respectively. The binding to these two integrins was tested to evaluate the *specificity* of the multivalent CNPs toward the integrin $\alpha_v\beta_3$. Significantly, all four CNP constructs demonstrated no specific binding toward the integrins $\alpha_v\beta_5$ and $\alpha_{IIb}\beta_3$, with
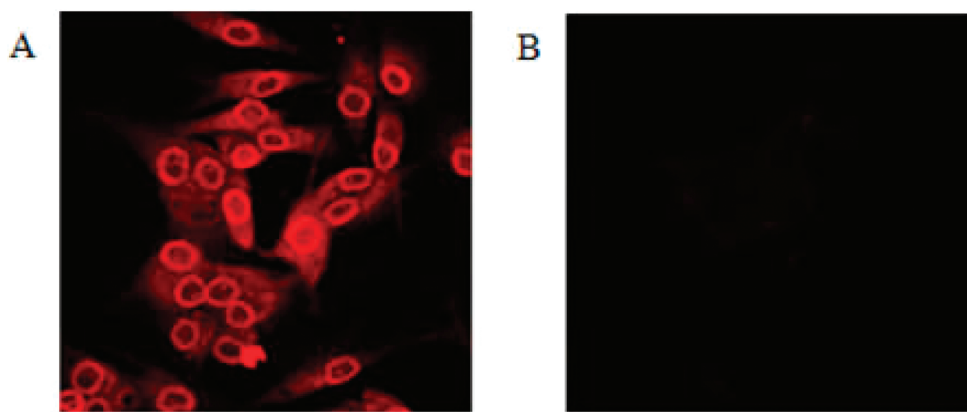
Figure 3. Confocal microscopy slides (red channel image) showing the internalization of 20% targeted CNPs in U87MG glioblastoma cells. The cells were incubated with respective nanoparticle solutions (143 nM) for 1 h at 37 °C. (A) Image showing accumulation of 20% RGD−comb nanoparticles into the cells. (B) Image showing no accumulation of 0% RGD−comb nanoparticles into the cells.
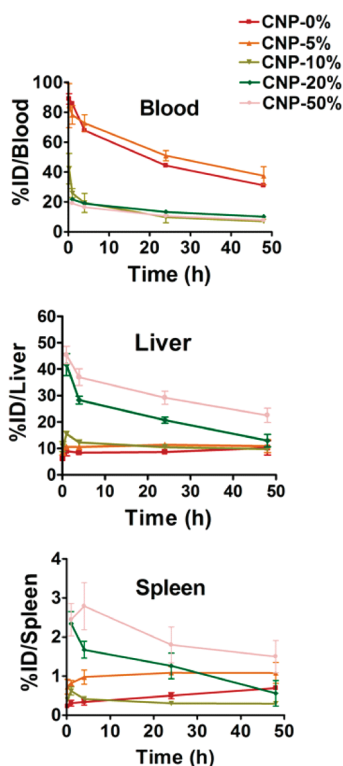
Figure 4. Blood (top), liver (middle), and spleen (bottom) retention profiles for the ^{64}Cu-labeled CNPs in Sprague−Dawley rats. Data are expressed as percent injected dose (% ID) per organ ± SD.

IC$_{50}$ values of >1000 nM. It should be noted that at higher concentrations weak binding was observed toward $\alpha_{IIb}\beta_3$. This is not surprising as modest binding would be expected to the β_3 part of the integrin; however, the near thousand-fold enhancement of binding toward $\alpha_v\beta_3$ when compared with $\alpha_v\beta_5$ and $\alpha_{IIb}\beta_3$ in all four RGD−CNP constructs suggests a high selectivity for $\alpha_v\beta_3$. It should also be noted that the small molecule analogue, GRGDS, was shown to have an IC$_{50}$ of 15.9, >5000, and 873 nM for $\alpha_v\beta_3$, $\alpha_v\beta_5$, and $\alpha_{IIb}\beta_3$,

respectively, displaying decreased selectivity when compared to the corresponding multivalent CNP. These results are promising for further application of these CNPs in clinical imaging and therapeutic settings.

Cell Uptake Assays. Cellular uptake assays were performed to evaluate the cellular uptake kinetics of the RGD−CNPs using $\alpha_v\beta_3$-positive U87MG human glioblastoma cells. The cellular associated radioactivity, which is the sum of the cell-internalized CNP fraction and cell surface-bound CNP fraction measured at a 30 min incubation time point and normalized to protein content, is presented in Figure 2. The 5, 10, and 20% RGD−CNPs demonstrated increasing internalization at 30 min post-incubation as the level of RGD functionalization increases, with average values of 10, 20, and 35% cell-associated fraction/mg protein, respectively. The 50% RGD−CNP demonstrated a slight decrease in cell uptake as compared to the 20% comb, with a value of about 30% cell-associated fraction/mg protein, suggesting an upper limit on the effect of increased RGD loading on cellular uptake efficiency, possibly due to the 50% RGD−CNP exceeding the optimal RGD peptide/integrin binding site ratio. Montet *et al.* have reasoned that this upper limit is reached when the density of RGD peptides on the CNP exceeds the density of RGD/integrin binding sites displayed by the cell membrane.[32] Because there is only one RGD binding site per integrin, the number of RGD peptides per CNP that participate in binding is limited by the number of integrins displayed by the membrane. Thus, any "extra" RGD peptides present on the multivalent nanoparticle cannot participate in integrin binding. Decuzzi *et al.* have argued that other key factors, such as the threshold particle radius, the optimal particle radius, and the characteristic wrapping time, may also play a role in the specific and nonspecific interactions in the receptor-mediated endocytic performances of nanometer particles.[33] The cellular uptake of the control peptide or the functionalized nanoparticles could be successfully blocked by the addition of an excess of the

corresponding nonradiolabeled peptide or CNP, respectively (Figure 2), consistent with the mechanism of receptor-mediated endocytosis of the RGD—CNPs.

Internalization Studies. The cellular uptake trend of the ^{64}Cu-labeled multivalent CNPs was clearly demonstrated by assays performed with the $\alpha_v\beta_3$-positive U87MG cells. Initial experiments to quantify the level of surface-bound CNPs *versus* internalized nanoparticles were complicated by strong adherence of the CNPs to the cell surface, preventing full removal by washing. In order to validate the internalization of the RGD—CNPs, confocal microscopy was therefore performed on the 20% RGD—CNP with $\alpha_v\beta_3$-positive U87MG cells. Since there was no fluorescent marker on the comb nanoparticle, the confocal imaging strategy involved targeting of the PEG units on the RGD—CNPs by a monoclonal anti-PEG antibody, which could be specifically detected by a fluorescent secondary marker. Significantly, the confocal images showed internalization of the 20% RGD—CNPs within 1 h of incubation with the cells (Figure 3), and the CNPs favored localization close to the perinuclear region inside the cell. The confocal images combined with the cellular studies using radioactive assays illustrate that high cellular uptake and internalization by receptor-mediated endocytosis can be achieved and manipulated through tuning of the nanoparticle structure.

Biodistribution Studies. Previous *in vivo* studies with nanoparticles bearing a targeting ligand (such as RGD, DNA aptamers, *etc.*) have shown that these moieties can lower the blood circulation lifetime and increase the immune response in comparison to nanoparticles that only have a PEG surface layer.[11,18] The structural control over nanoparticle size and peptide loading coupled with the ability to introduce diagnostic units permits the *ex vivo* results described above to be compared with the *in vivo* pharmokinetic behavior of the multivalent CNPs. Toward this aim, ^{64}Cu-labeled CNPs with varying loadings of RGD were administered intravenously to normal rats, with blood retention, liver, and spleen accumulation studied in detail.

The blood retention profiles for the RGD—CNP series are shown in Figure 4. The 10, 20, and 50% RGD—CNPs demonstrate relatively fast blood clearance to 1 h followed by stabilization of blood activity to 48 h. In contrast, the 5% RGD—CNPs exhibit a similar blood retention profile as the control particle without RGD, with the blood retention remaining high out to 48 h. These results show that, for the GRGDS ligand, low loadings have minimal effect on blood retention while higher loadings drastically decrease blood retention.

There was no significant accumulation in the lungs, as expected from non-aggregating nanoparticles.

We monitored the liver and spleen uptake of the CNPs as the liver contains some of the principal phagocytic cells (*e.g.*, Kupffer cells, hepatocytes, hepatic stellate cells) and both organs eliminate foreign particulate, macromolecules, and senescent cells.[34] The liver and spleen uptake for our series of nanoparticles is shown in Figure 4 (middle and bottom panel). Both the 20 and 50% RGD—CNPs are quickly uptaken by the liver and spleen, and their concentrations slowly decrease presumably *via* urinary and fecal excretion, as increased excretion is seen for the RGD—CNPs (data not shown), whereas the 0, 5, and 10% RGD—CNPs show only moderate uptake in the liver and spleen. These results reveal that increases in the amount of RGD on a CNP surface can lead to a greater response from the RES of an organism. Future studies will examine different peptide sequences for targeting integrins in order to understand the effect of the nature of the peptide (hydrophilic/hydrophobic, charge, *etc.*) combined with its loading level and structural position on the biodistribution.

CONCLUSIONS

The tunable and modular synthesis of functionalized comb copolymers has enabled facile development of a library of multivalent nanoparticles incorporating diagnostic [64]Cu—DOTA units with varying amounts of surface-accessible RGD peptides for $\alpha_v\beta_3$ targeting. By controlling the level of targeting moieties, while maintaining similar nanoparticle sizes, fundamental structure/bioperformance relationships were developed and the effects of functional group density on pharmacological profiles and biological behavior explored. The *in cellulo* results indicate an upper limit of RGD loading for effective cellular uptake in $\alpha_v\beta_3$-positive U87MG glioblastoma cells, while the *in vivo* results show a balance between the level of targeting ligand and biodistribution. This ability to screen a library of well-defined nanoparticles is critical in designing the optimal material parameters for therapeutic and imaging applications while at the same time developing a fundamental understanding of the interaction of functionalized nanoparticles with cellular and *in vivo* systems. The lessons learned from model $\alpha_v\beta_3$-targeted CNPs can thus be applied for a variety of molecular targets and targeting ligands using the CNP nanoparticle scaffold.

EXPERIMENTAL SECTION

Materials. Chemicals were purchased from Sigma-Aldrich (St. Louis, MO) and used without further purification unless

otherwise stated, and functionalized poly(ethylene glycol) (PEG) derivatives were obtained from Intezyne Technologies, (Tampa, FL). [64]Cu was prepared on the Washington University Medical

School CS-15 Cyclotron by the $^{64}Ni(p,n)^{64}Cu$ nuclear reaction at a specific activity of 50–200 mCi/μg (end of bombardment), as previously described.[35] The buffers used for ^{64}Cu labeling were treated with Chelex-100 resin (Bio-Rad Laboratories, Hercules, CA) before use. Tris-*t*-butylester-DOTA and 1,4,7,10-tetraazacyclododecane were purchased from Macrocyclics (Dallas, TX). Centricon tubes (YM-30, MWCO = 30 kDa; YM-50, MWCO = 50 kDa; YM-100, MWCO = 100 kDa) were purchased from Millipore. HiTrap desalting columns (5 mL) were purchased from GE Healthcare Biosciences (Piscataway, NJ). 2-(2-Bromoacetoxy-)ethyl methacrylate,[36] dithiolester radical addition–fragmentation transfer (RAFT) agent,[37] 1,4,7,10-tetraazacyclododecane-1,4,7-tris(*t*-butyl acetate) (DO3A),[38] and 4-pentynoic anhydride[39] were prepared as previously reported. Vitronectin, fibronectin, $\alpha_v\beta_3$, and $\alpha_v\beta_5$ were purchased from Chemicon. Integrin $\alpha_{IIb}\beta_3$ was purchased from EMD Chemicals, Inc. (Gibbstown, NJ).

Polymeric materials were characterized by ^1H and ^{13}C nuclear magnetic resonance (NMR) spectroscopy using either a Bruker 200, 300, or 500 MHz spectrometer with the residual solvent signal as an internal reference. Gel permeation chromatography (GPC) was performed in DMF on a Waters system (Millford, MA) equipped with four 5 mm Waters columns (300 × 7.7 mm) connected in series with increasing pore size (10^2, 10^3, 10^4, and 10^6 Å). Waters 410 differential refractometer index and 996 photodiode array detectors were employed. The molecular weights of the polymers were calculated relative to linear poly(ethylene oxide) standards. Fourier transformed infrared spectroscopy was performed using a Nicolet Magna 850 IR-Raman instrument on a CaF_2 salt plate. The spectra were acquired at a 4 cm^{-1} resolution and 128 scans. A Bioscan 200 imaging scanner (Bioscan, Washington, DC) was used to read the instant thin layer chromatography (ITLC) plates (Pall ITLC-SG plates, VWR International, Batavia, IL). Fast protein liquid chromatography (FPLC) and radio-FPLC were performed using an AKTA FPLC system (GE Healthcare Biosciences) equipped with a Beckman 170 radioisotope detector (Beckman Instruments, Fullerton, CA).

Synthesis of DOTA Methacrylate (DOTA-MA) (3). DO3A (1.92 g, 3.74 mmol) and 2-(2-bromoacetoxy)ethyl methacrylate (1.02 g, 4.06 mmol) were dissolved in acetonitrile (50 mL) followed by the addition of K_2CO_3 (0.62 g, 4.48 mmol), and the reaction mixture was then stirred overnight at room temperature. Dichloromethane (50 mL) was added to the reaction which was extracted with water (25 mL), concentrated by rotary evaporation, and purified by flash chromatography (DCM/MeOH, 95:5) to obtain a viscous clear oil (yield 1.81 g, 71%): ^1H NMR (500 MHz, CDCl$_3$) δ 6.14 (s, 1H), 5.63 (s, 1H), 4.39 (d, J = 19.1 Hz, 4H), 3.98–2.05 (m, 22H), 1.96 (s, 3H), 1.47 (t, J = 6.7 Hz, 27H). The product was anayzed with ESI-TOF mass spectrometry: (m/z) [M]$^+$ calcd 684.43, $C_{34}H_{60}N_4O_{10}$; found 684.53.

Synthesis of Poly(ethylene glycol)methyl ether methacrylate (PEGMA). Poly(ethylene glycol) monomethyl ether (5.0 kDa, mPEG, 5.00 g, 1.00 mmol) was dissolved in dichloromethane (25 mL) and triethylamine (5 mL). Freshly distilled methacryloyl chloride (5.00 mL, 5.35 g, 5.12 mmol) was added dropwise at 0 °C, and the reaction mixture was allowed to stir overnight under argon. The reaction was quenched with water, filtered, and the organic phase washed with 10% $NaHSO_4$ (w/v), dried over anhydrous $MgSO_4$, and concentrated in vacuum to *ca.* 10 mL. The product was precipitated by adding cold diethyl ether (200 mL) and dried in vacuum (4.65 g, 92%): ^1H NMR (CDCl$_3$, 200 MHz) δ 6.15 (1H), 5.58 (1H), 4.32 (2H), 3.6 (450H), 1.95 (2H); M_n = 5.1 kDa; PDI = 1.03.

Synthesis of Azidopoly(ethylene glycol)methacrylate (N$_3$-PEGMA) (4). Poly(ethylene glycol)monoazide (5.0 kDa, 1.50 g, 0.30 mmol) was dissolved in dichloromethane (15 mL) and triethylamine (3 mL). Freshly distilled methacryloyl chloride (0.70 mL, 0.75 g, 7.1 mmol) was added dropwise at 0 °C, and the reaction mixture was allowed to stir overnight under argon. The reaction was quenched with water, filtered, and the organic phase washed with 10% $NaHSO_4$ (w/v), dried over anhydrous $MgSO_4$, and concentrated in vacuum to *ca.* 3 mL. The product was precipitated by adding cold diethyl ether (100 mL) and dried in vacuum (yield 1.11 g, 74%): ^1H NMR (500 MHz, CD$_2$Cl$_2$) δ 6.13

(s, 1H), 5.61 (s, 1H), 4.35–4.26 (m, 2H), 3.78–3.57 (m, 464H), 3.53–3.45 (m, 3H), 3.42 (t, J = 5.0 Hz, 2H), 1.97 (s, 3H); M_n = 5.1 kDa; PDI = 1.03.

Synthesis of Acteylene GRGDS (5). GRGDS (145 mg, 0.30 mmol) was dissolved in 1.5 mL of anhydrous DMF and 4-pentynoic anhydride (66.5 mg, 0.37 mmol) dissolved in 0.5 mL of anhydrous DMF added dropwise to the solution and allowed to stir overnight. Cold diethyl ether (20 mL) was added to the solution to triturate the product, which was subsequently dissolved in 2 mL of Milli-Q water and freeze-dried (yield 132 mg, 78%): ^1H NMR (500 MHz, DMSO) δ 8.28 (s, 1H), 8.22 (s, 1H), J = 7.8 Hz, 1H), 8.14 (t, J = 5.6 Hz, 1H), 8.04 (d, J = 7.7 Hz, 1H), 7.83 (d, J = 6.4 Hz, 1H), 4.64 (dd, J = 13.1, 7.7 Hz, 1H), 4.29 (dd, J = 13.4, 7.6 Hz, 1H), 4.24–4.16 (m, 1H), 3.84–3.67 (m, 5H), 3.63 (dd, J = 11.1, 4.2 Hz, 1H), 3.09 (d, J = 6.0 Hz, 3H), 2.36 (s, 4H), 1.74 (s, 1H). The product was anayzed with ESI-TOF mass spectrometry: (m/z) [M]$^+$ calcd 570.24, $C_{22}H_{34}N_8O_{10}$; found 570.33.

Synthesis of Poly(ethylene glycol) GRGDS Methacrylate (RGD-PEGMA) (6). N$_3$-PEGMA (323 mg, 0.065 mmol) and acetylene GRGDS (64 mg, 0.11 mmol) were dissolved in a solution of 1.82 g of DMSO and 1.27 g of Milli-Q water followed by the additions of aqueous CuSO$_4$ (60 μL, 0.018 mmol, 5 wt %) and aqueous Na-ascorbate (75 μL, 0.16 mmol, 5 wt %), respectively. The reaction was allowed to stir for 2 days with additions of CuSO$_4$ (60 μL, 5 wt %) and Na-ascorbate (75 μL, 5 wt %) after 1 day. The product was purifted by washing (10×) with Milli-Q water in 15 mL centricon tubes (YM-5) and freeze-dried (yield 323 mg, 90%): ^1H NMR (500 MHz, DMSO) δ 8.62 (s, 1H), 8.46–8.40 (m, 1H), 7.82 (s, 1H), 7.36 (s, 1H), 6.95 (s, 1H), 6.04 (s, 1H), 5.69 (d, J = 1.6 Hz, 1H), 4.46 (d, J = 5.0 Hz, 3H), 4.29–4.16 (m, 3H), 3.53 (d, J = 16.2 Hz, 524H), 2.85 (t, J = 7.5 Hz, 3H), 1.90 (t, J = 6.7 Hz, 3H); M_n = 5.4 kDa; PDI = 1.05.

Synthesis of Comb Copolymers. The synthesis of comb polymers was adapted from a previous report[28] with the exception of DOTA methacrylate and poly(ethylene glycol) GRGDS methacrylate being incorporated into the polymerization mixture. To illustrate with the 10% RGD comb: PEGMA 5.0 kDa (147 mg, 0.029 mmol), RGD-PEGMA (40 mg, 0.0072 mmol), methyl methacrylate (MMA) (29.2 mg, 0.29 mmol), azobisisobutyronitrile (AIBN) (0.024 mg, 0.00015 mmol), DOTA-MA (14.8 mg, 0.022 mmol), and RAFT agent (0.22 mg, 0.00073 mmol) were dissolved in DMF (516 mg). AIBN, DOTA-MA, and RAFT agent were added as DMF stock solutions. The solution was transferred to a 2 mL Schlenk flask, and three freeze–pump–thaw cycles were performed before being heated at 70 °C for 48 h. Following the polymerization, the solution was diluted with DMF, transferred to four 15 mL centricon tubes (YM-50), and extensively washed with DMF. The copolymer was then washed with Milli-Q water (5×) and freeze-dried to give the desired graft copolymer as a white powder (yield 41 mg): ^1H NMR (500 MHz, DMSO) δ 3.91–3.39 (m, $-OCH_2CH_2O-$), 2.05–1.64 (s, $-CH_3$), 1.55–1.38 (s, t-$C(CH_3)_3$), 1.05–0.59 (d, $-CH_2-$); M_n = 130 kDa; PDI = 1.3.

DOTA Deprotection and Formation of CNPs. The *t*-butyl groups of the DOTA functional groups of the copolymers were deprotected with a 9:1 v/v mixture of dichloromethane/trifluoroacetic acid (TFA). Representatively, the 5% RGD comb copolymer (18 mg) was dissolved in dichloromethane/TFA (9/1 v/v, 1 mL) and stirred overnight at room temperature. After solvent removal, the oily residue was redissolved in dichloromethane (1 mL) and precipitated in hexane (25 mL). This procedure was repeated three times followed by drying in vacuum. The obtained product was dissolved in dimethylsulfoxide (DMSO) (1% w/v), and then an equal volume of water was added in one aliquot. The solution was stirred for 2–3 h, and DMSO was then removed by centrifugal filtration. After centrifugal filtration cycles with Milli-Q water (3×), the CNPs were reconstituted in water (*ca.* 3 mg/mL) and stored at 4 °C for further use.

Dynamic Light Scattering (DLS). DLS measurements were carried out on a Brookhaven BI-9000AT Digital Autocorrelator (Holtsville, NY) equipped with an Avalanche photodiode detector and a MG vertically polarized 35 mmV helium–neon 633 nm laser and operated by the 9KDLSW control program. All samples were filtered through 0.45 μm and run in triplicate for 10 min at 25 °C, at 1 mg/mL, and at a fixed 90° angle. Hydrodynamic diameter and distribution of particles were determined by

fitting the correlation functions with the ISDA analysis software package (Brookhaven Instruments Co.) and applying the non-negatively constrained least-squares particle size distribution analysis (NNLS).[40]

Radiolabeling of DOTA-CNPs with ^{64}Cu. ^{64}Cu chloride (5−10 μL in 0.5 M HCl) was diluted with 0.1 M ammonium acetate buffer (pH 5.5, 50−100 μL). The CNP solutions (3 mg/mL, 30−200 μL) were two-fold diluted with acetate buffer, ^{64}Cu-acetate (2−5 mCi) was added, and the mixture was incubated at 80 °C for 1 h. Following radiolabeling of the CNPs, 5−10 μL of 10 mM aqueous ethylenediamine tetraacetic acid (EDTA) solution was added and incubation continued for another 10 min at room temperature (RT) with the labeling yield determined by radio-iTLC using a 1:1 mixture (v/v) of 10 wt % ammonium acetate and methanol as eluent (R_f = 0 for the labeled product and R_f = 0.9 for the free ^{64}Cu and/or ^{64}Cu-EDTA complex). Zeba desalting spin columns (2 mL, Pierce) were used to separate the radiolabeled products from the residual free ^{64}Cu and/or ^{64}Cu-EDTA complex. After purification, the radiochemical purity (RCP) of the ^{64}Cu-labeled CNPs was monitored by radio-FPLC. The products were then diluted with binding buffer (pH 7.4) to prepare appropriate doses for cell studies or with PBS for biodistribution studies.

In vitro stability of the ^{64}Cu-labeled nanoparticles was evaluated by incubating the compounds in both PBS and mouse serum and by analyzing aliquots by radio-iTLC at different time points up to 48 h.

The number of DOTA groups available to chelate the Cu was estimated by adding 100 μg of the nanoparticles to a known excess of "hot plus cold" Cu-acetate (a nonradioactive Cu-acetate solution spiked with 50−100 μCi ^{64}Cu). After 1 h incubation at 80 °C, a 10 mM aqueous ethylenediamine tetraacetic acid (EDTA) was added and the resulting solution was incubated for 10 min at RT. Aliquots (2 μL) were then analyzed by radio-iTLC: the ^{64}Cu-labeled nanoparticles remained at the origin while the ^{64}Cu-EDTA complex migrated with an R_f of 0.9. The number of DOTA chelates attached to the comb copolymers was determined from the counts per minute (cpm) in the radio chromatogram, with the following equation:

$$n(\text{chelates}) = \frac{n(\text{copper}) \times \text{cpm}(R_f < 0.3)}{\text{cpm}(\text{total})}$$

FPLC Analysis. An aliquot (100 μL, *ca.* 15 μCi) of the ^{64}Cu-labeled CNPs was injected into a Superose 12 gel filtration column (GE Healthcare Biosciences) and eluted with 20 mM HEPES and 150 mM NaCl (pH 7.3) at 0.8 mL/min. The UV wavelength was preset to 280 nm, and the radioactivity was monitored by an in-line radio detector. Under these conditions, the retention times of the native and radiolabeled nanoparticles were 8−10 mL while the retention times of free ^{64}Cu and ^{64}Cu-EDTA were 20−22 mL. Samples with RCP > 95% were used for cells or animal studies.

Biodistribution Studies. All animal studies were performed in compliance with guidelines set by the Washington University Animal Studies Committee. Normal female Sprague−Dawley rats (180−200 g, n = 4 per time point) anesthetized with 1−2% vaporized isoflurane and injected *via* the tail vein with approximately 15 μCi in 200 μL of PBS (80−100 μg/kg rat body weight). At each time point, the rats were anesthetized prior to sacrifice. Organs of interest were removed and blotted dry. The activity was measured in a gamma counter. The total activity in the blood was calculated assuming 6% of the rat body weight.[41] Diluted standard doses (1:100) were prepared and counted along with the samples. All of the data were corrected for ^{64}Cu decay. The percent injected dose per gram of tissue (%ID/g) values were calculated using the following equation:

$$\%\text{ID/g}$$
$$= \frac{(\text{cpm in sample} - \text{background}) \times 10^2}{(\text{decay correction factor}) \times (\text{sample weight}) \times (\text{cpm in standard})}$$

Cell Culture. All cell handling was aseptically performed in a laminar flow hood. U87MG human glioblastoma cell lines were purchased from the American Tissue Culture Collection and were grown until 60−75% confluency in T75 tissue culture flasks. The cells were maintained at a concentration of 1×10^6 cells/mL in Iscove's modified Dulbeccos's medium (GIBCO-BRL) at 37 °C in a humidified atmosphere with 5% CO$_2$ in a Revco Elite II incubator. To determine cell density, equal amounts of cell suspension and trypan blue exclusion were added to a hemocytometer to calculate a cells/mL concentration and ensure cell viability.

Competitive Binding Assay. The 96-well plates (Nunc Immuno Plate with MaxiSorp) were coated with 100 μL of human integrin $\alpha_v\beta_3$ or $\alpha_v\beta_5$ (Chemicon Intl., Inc.) or $\alpha_{IIb}\beta_3$ (EMD Chemicals) (1 μg/mL) in coating buffer (20 mM Tris, pH 7.4, 150 mM NaCl, 2 mM CaCl$_2$, 1 mM MgCl$_2$, 10 μM MnCl$_2$) for 1 h at 4 °C. The plates were then blocked with blocking buffer (3% BSA in coating buffer; 200 μL per well) for 1 h at 4 °C. After washing the plates three times with binding buffer (0.1% BSA in coating buffer), serially diluted test CNP solutions were added along with 14 nM biotinylated vitronectin solution for integrins $\alpha_v\beta_3$ and $\alpha_v\beta_5$ and 14 nM biotinylated fibronectin for integrin $\alpha_{IIb}\beta_3$. Biotinylated vitronectin or fibronectin (chemicon) was prepared by using sulfo-biotin-NHS (Pierce Biotechnology). The reagents were allowed to bind to the respective integrins for 2 h at 37 °C. Following incubation, the plates were washed three times with the binding buffer to remove unbound reagents. Bound biotinylated vitronectin/fibronectin was detected by adding ExtrAvidin alkaline phosphatase conjugate (Sigma) (1/35 000 dilution, 1 h, RT) using the *p*-nitrophenyl phosphate substrate solution as the chromogen (30 min, RT, in dark). Absorbance was read on the spectrophotometer at 405 nm. Each concentration data point was evaluated in triplicate, and nonspecific binding was subtracted from each data point. Nonlinear regression was used to fit binding curves and calculate IC$_{50}$ values (Prism, version 4.0, GraphPad). A control assay with a small peptide whose IC$_{50}$ was previously known (*e.g.*, c(RGDyK), IC$_{50}$ 3.7 nM) was always run concurrently with the test assay to validate the accuracy of procedure and reagents.

Cellular Uptake/Internalization Assay. U87MG human glioblastoma cells were grown in Iscoves MDM until 60−75% confluent. The cells were harvested by mechanical dissociation and resuspended in the binding medium (Iscoves MDM, 1% glutamine, 1% BSA, 0.1 mM Mg^{2+} and 0.1 mM Mn^{2+}) in microfuge tubes. The ^{64}Cu-labeled nanoparticle solution (1 nM, 20−50 uL) was added to the cell suspension. The samples were incubated for 0, 30, and 60 min in a cell incubator (37 °C, 5% CO$_2$). For blocking experiments, the samples were co-incubated with 1 μM nonradioactive nanoparticle solution (500 μL total volume). After incubation, the samples were centrifuged at 1400 rpm for 1 min, and the radioactive medium was removed. Cell pellets were rinsed with ice cold binding buffer (500 μL) and centrifuged at 1400 rpm for 1 min (2×). The surface-bound fraction was collected by suspending the cells in 500 μL strip buffer (5% Trypsin EDTA, pH 7.4), followed by incubation for 10 min at 37 °C. The cells were separated *via* centrifugation followed by one more washing with 500 μL strip buffer. The combined strip-buffer wash fractions constituted the surface-bound fraction. The radioactivity in each fraction was measured in a well counter (Packard II gamma counter). The protein content of each cell lysate sample was determined (BCA Protein Assay Kit, Pierce) to normalize the data.

Microscopy. The U87MG cells were plated on tissue culture treated glass slides and incubated with 20% comb nanoparticles for 1.5 h at 37 °C. Following incubation, the unbound nanoparticles were washed off, and the cells were fixed with 4% paraformaldehyde (PFA) solution and permeabilized with 0.2% Triton X-100 in PBS. Following fixation and permeabilization steps, PEG monoclonal antibody (20 μg/mL; Biodesign, Catalog #G01237M, Clone B141M; 30 min; 37 °C) was added to react with PEG units present on the internalized CNPs. After removal of the unbound antibody and washings with PBS (4×), secondary reagent for detecting the PEG antibody was added (Invitrogen; SKU# A-21237; Alexa Fluor 647 F(ab')$_2$ fragment of goat anti-mouse IgG (H+L); 2 mg/mL; 1/100 dilution; 20 min; RT). Final step involved washing off of any unbound reagent (PBS, 4×) and placing of mounting media before coverslipping the slide. Confocal images were collected 24 h later with an Olympus FV1000 microscope using a 60×/1.20 M, 0.13−0.21 NA water immersion objective. Fluorescence emission was detected

by using a 633 nm laser at 15% transmission and 655—700 nm emission.

REFERENCES AND NOTES

1. Lu, W.; Arumugam, S. R.; Senapati, D.; Singh, A. K.; Arbneshi, T.; Khan, S. A.; Yu, H.; Paresh, C. R. Multifunctional Oval-Shaped Gold-Nanoparticle-Based Selective Detection of Breast Cancer Cells Using Simple Colorimetric and Highly Sensitive Two-Photon Scattering Assay. *ACS Nano* **2010,** *4,* 1739–1749.

2. Xu, H.; Minoia, A.; Tomović, Z.; Lazzaroni, R.; Meijer, E. W.; Schenning, A. P. H. J.; De Feyter, S. A Multivalent Hexapod: Conformational Dynamics of Six-Legged Molecules in Self-Assembled Monolayers at a Solid—Liquid Interface. *ACS Nano* **2009,** *3,* 1016–1024.

3. Kumar, A. M. S.; Sivakova, S; Fox, J. D.; Green, J. E.; Marchant, R. E.; Rowan, S. J. Molecular Engineering of Supramolecular Scaffold Coatings That Can Reduce Static Platelet Adhesion. *J. Am. Chem. Soc.* **2008,** *130,* 1466–1476.

4. Sudeep, P. K.; Emrick, T. Functional Si and CdSe Quantum Dots: Synthesis, Conjugate Formation, and Photoluminescence Quenching by Surface Interactions. *ACS Nano* **2009,** *3,* 4105–4109.

5. Liu, J.; Zhang, Q.; Remsen, E. E.; Wooley, K. L. Nanostructured Materials Designed for Cell Binding and Transduction. *Biomacromolecules* **2001,** *2,* 362–368.

6. Ostaci, R.-V.; Damiron, D.; Grohens, Y.; Léger, L.; Drockenmuller, E. Click Chemistry Grafting of Poly(ethylene glycol) Brushes to Alkyne-Functionalized Pseudobrushes. *Langmuir* **2010,** *26,* 1304–1310.

7. Zareie, H. M.; Boyer, C.; Bulmus, V.; Nateghi, E.; Davis, T. P. Temperature-Responsive Self-Assembled Monolayers of Oligo(ethylene glycol): Control of Biomolecular Recognition. *ACS Nano* **2008,** *2,* 757–765.

8. Stukel, J. M.; Li, R. C.; Maynard, H. D.; Caplan, M. R. Two-Step Synthesis of Multivalent Cancer-Targeting Constructs. *Biomacromolecules* **2010,** *11,* 160–167.

9. Zhang, L.; Gu, F. X.; Chan, J. M.; Wang, A. Z.; Langer, R. S.; Farokhzad, O. C. Nanoparticles in Medicine: Therapeutic Applications and Developments. *Clin. Pharmacol. Ther.* **2008,** *83,* 761–769.

10. Wagner, V.; Dullaart, A.; Bock, A. K.; Zweck, A. The Emerging Nanomedicine Landscape. *Nat. Biotechnol.* **2006,** *24,* 1211–1217.

11. Almutairi, A.; Rossin, R.; Shokeen, M.; Hagooly, A.; Ananth, A.; Capoccia, B.; Guillaudeu, S.; Abendschein, D.; Anderson, C. J.; Welch, M. J.; *et al.* Biodegradable Dendritic Positron-Emitting Nanoprobes for the Noninvasive Imaging of Angiogenesis. *Proc. Natl. Acad. Sci. U.S.A.* **2009,** *106,* 685–690.

12. Torchilin, V. P. Micellar Nanocarriers: Pharmaceutical Perspectives. *Pharm. Res.* **2007,** *24,* 1–16.

13. El Bayoumi, T. A.; Torchilin, V. P. Tumor-Targeted Nanomedicines: Enhanced Antitumor Efficacy *In Vivo* of Doxorubicin-Loaded, Long-Circulating Liposomes Modified with Cancer-Specific Monoclonal Antibody. *Clin. Cancer Res.* **2009,** *15,* 1973–1980.

14. Glickson, J. D.; Lund-Katz, S.; Zhou, R.; Choi, H.; Chen, I. W.; Li, H.; Corbin, I.; Popov, A. V.; Cao, W.; Song, L.; *et al.* Lipoprotein Nanoplatform for Targeted Delivery of Diagnostic and Therapeutic Agents. *Adv. Exp. Med. Biol.* **2009,** *645,* 227–239.

15. Nahrendorf, M.; Zhang, H.; Hembrador, S.; Panizzi, P.; Sosnovik, D. E.; Aikawa, E.; Libby, P.; Swirski, F. K.; Weissleder, R. Nanoparticle PET-CT Imaging of Macrophages in Inflammatory Atherosclerosis. *Circulation* **2008,** *117,* 379–387.

16. Prato, M.; Kostarelos, K.; Bianco, A. Functionalized Carbon Nanotubes in Drug Design and Discovery. *Acc. Chem. Res.* **2008,** *41,* 60–68.

17. Johnston, A. P. R.; Cortez, C.; Angelatos, A. S.; Caruso, F. Layer-by-Layer Engineered Capsules and Their Applications. *Colloid Interface Sci.* **2006,** *11,* 203–209.

18. Gu, F.; Zhang, L.; Teply, B. A.; Mann, N.; Wang, A.; Radovic-Moreno, A. F.; Langer, R.; Farokhzad, O. C. Precise Engineering of Targeted Nanoparticles by Using Self-Assembled Biointegrated Block Copolymers. *Proc. Natl. Acad. Sci. U.S.A.* **2008,** *105,* 2586–2591.

19. Shokeen, M.; Fettig, N. M.; Rossin, R. Synthesis, *In Vitro* and *In Vivo* Evaluation of Radiolabeled Nanoparticles. *J. Nucl. Med. Mol. Imaging* **2008,** *52,* 267–277.

20. Hood, J. D.; Cheresh, D. A. Role of Integrins in Cell Invasion and Migration. *Nat. Rev. Cancer* **2002,** *2,* 91–100.

21. Moghimi, S. M.; Hunter, A. C.; Murray, J. C. Long-Circulating and Target-Specific Nanoparticles: Theory to Practice. *Pharmacol. Rev.* **2001,** *53,* 283–318.

22. Owens, D. E., III; Peppas, N. A. Opsonization, Biodistribution, and Pharmacokinetics of Polymeric Nanoparticles. *Int. J. Pharm.* **2006,** *307,* 93–102.

23. Lutz, J. F. 1,3-Dipolar Cycloadditions of Azides and Alkynes: A Universal Ligation Tool in Polymer and Materials Science. *Angew. Chem., Int. Ed.* **2007,** *46,* 1018–1025.

24. Parrish, B.; Breitenkamp, R. B.; Emrick, T. PEG- and Peptide-Grafted Aliphatic Polyesters by Click Chemistry. *J. Am. Chem. Soc.* **2005,** *127,* 7404–7410.

25. Vestberg, R.; Piekarski, A. M.; Pressly, E. D.; Van Berkel, K. Y.; Malkoch, M.; Gerbac, J.; Ueno, N.; Hawker, C. J. A General Strategy for Highly Efficient Nanoparticle Dispersing Agents Based on Hybrid Dendritic Linear Block Copolymers. *J. Polym. Sci., Part A: Polym. Chem.* **2009,** *47,* 1237–1258.

26. Dechantsreiter, M. A.; Planker, E.; Matha, B.; Lohof, E.; Holzemann, G.; Jonczyk, A.; Goodman, S. L.; Kessler, H. N-Methylated Cyclic RGD Peptides as Highly Active and Selective Alpha(V)Beta(3) Integrin Antagonists. *J. Med. Chem.* **1999,** *42,* 3033–3040.

27. Fiamengo, A. L. Y., Y; Achilefu, S.; Anderson, C. J. *In Vitro* and *In Vivo* Evaluation of Structurally Diverse Cu-64-Labeled RGD Peptides for PET Imaging of Alpha V Beta 3 Expression. *J. Labelled Compd. Radiopharm.* 2009, 52.

28. Pressly, E. D.; Rossin, R.; Hagooly, A.; Fukukawa, K.; Messmore, B. W.; Welch, M. J.; Wooley, K. L.; Lamm, M. S.; Hule, R. A.; Pochan, D. J.; *et al.* Structural Effects on the Biodistribution and Positron Emission Tomography (PET) Imaging of Well-Defined (64)Cu-Labeled Nanoparticles Comprised of Amphiphilic Block Graft Copolymers. *Biomacromolecules* **2007,** *8,* 3126–3134.

29. Alb, A. M.; Enohnyaket, P.; Drenski, M. F.; Shunmugan, R.; Tew, G. N.; Reed, W. F. Quantitative Contrasts in the Copolymerization of Acrylate- and Methacrylate-Based Comonomers. *Macromolecules* **2006,** *39,* 8283–8292.

30. Rodlert, M.; Harth, E.; Rees, I.; Hawker, C. J. End-Group Fidelity in Nitroxide-Mediated Living Free-Radical Polymerizations. *J. Polym. Sci., Part A: Polym. Chem.* **2000,** *38,* 4749–4763.

31. Wang, D.; Miller, S. C.; Sima, M.; Parker, D.; Buswell, H.; Goodrich, K. C.; Kopečková, P.; Kopeček, J. The Antrotropism of Macromolecules in Adjuvant-Induced Arthritis Rat Model: A Prelimary Study. *Pharm. Res.* **2004,** *21,* 1741–1749.

32. Montet, X.; Funovics, M.; Montet-Abou, K.; Weissleder, R.; Josephson, L. Multivalent Effects of RGD Peptides Obtained by Nanoparticle Display. *J. Med. Chem.* **2006,** *49,* 6087–6093.

33. Decuzzi, P.; Ferrari, M. The Role of Specific and Non-Specific Interactions in Receptor-Mediated Endocytosis of Nanoparticles. *Biomaterials* **2007,** *28,* 2915–2922.

34. Popielarski, S. R.; Hu-Lieskovan, S.; French, S. W.; Triche, T. J.; Davis, M. E. A Nanoparticle-Based Model Delivery System to Guide the Rational Design of Gene Delivery to the Liver. 2. *In Vitro* and *In Vivo* Uptake Results. *Bioconjugate Chem.* **2005,** *16*, 1071–1080.

35. McCarthy, D. W.; Shefer, R. E.; Klinkowstein, R. E.; Bass, L. A.; Margeneau, W. H.; Cutler, C. S.; Anderson, C. J.; Welch, M. J. Efficient Production of High Specific Activity [64]Cu Using a Biomedical Cyclotron. *Nucl. Med. Biol.* **1997,** *24*, 35–43.

36. Kilcher, G.; Wang, L.; Duckham, C.; Tirelli, N. Polysulfide Networks. *In Situ* Formation and Characterization of the Elastomeric Behavior. *Macromolecules* **2007,** *40*, 5141–5149.

37. Sébastien, P.; Pittaya, T. Macromolecular Design *via* Reversible Addition-Fragmentation Chain Transfer (RAFT)/Xanthates (MADIX) Polymerization. *J. Polym. Sci., Part A: Polym. Chem.* **2005,** *43*, 5347–5393.

38. Faulkner, S.; Burton-Pye, B. P. pH Dependent Self-Assembly of Dimetallic Lanthanide Complexes. *Chem. Commun.* **2005,** 259–261.

39. Malkoch, M.; Schleicher, K.; Drockenmuller, E.; Hawker, C. J.; Russell, T. P.; Wu, P.; Fokin, V. V. Structurally Diverse Dendritic Libraries: A Highly Efficient Functionalization Approach Using Click Chemistry. *Macromolecules* **2005,** *38*, 3663–3678.

40. Morrison, I. D.; Grabowski, E. F.; Herb, C. A. Improved Techniques for Particle Size Determination by Quasi-Elastic Light Scattering. *Langmuir* **1985,** *1*, 496–501.

41. Lee, H. B.; Blaufox, M. D. Blood Volume in the Rat. *J. Nucl. Med.* **1985,** *25*, 72–76.